scientific reports

Check for updates

OPEN

Fluctuating soil salinity across natural and managed landscapes of the coastal mid-Atlantic facing rapid sea-level rise

Manan Sarupria[1]✉, Rodrigo Vargas[2,3], Taejin Park[4,5] & Pinki Mondal[1,2]

The coastal mid-Atlantic region of the United States is increasingly vulnerable to soil salinization, primarily driven by sea-level rise and powerful coastal storms, posing a threat to farmland productivity, and ecological stability. However, the spatially heterogeneous nature of salinization across different land covers makes it challenging to monitor their interactions across large areas and longer time periods. To address this gap, we combined remote sensing-based land cover classification with modeled soil salinity data to assess landscape-scale dynamics across the Delmarva Peninsula from 2000 to 2016. Using a Random Forest classifier trained on Continuous Change Detection and Classification (CCDC)-derived synthetic Landsat surface reflectance, we generated gridded land cover datasets for five years (2000, 2002, 2005, 2009, and 2016) to match and compare with the existing Global Soil Salinity Maps. Overall, forests and other vegetation expanded, whereas farmland and bare soil declined. Salinization trend across these land covers is neither uniformly optimistic nor categorically alarming. Our results showed that over 75% of Delmarva remained in the non-saline category in those 5 years, increasing by 1,138 km², and extremely saline zones declined by 833 km². More than 83% of land cover transitions occurred without changing salinity categories, while 7–11% moved to a lower salinity category. Our findings based on these temporal snapshots reveal fluctuations in salinity across different land covers, underscoring the value of multi-temporal remote sensing for continuous monitoring of salinity-driven land changes.

Keywords Continuous Change Detection and Classification (CCDC), Delmarva Peninsula, Land cover change, Saltwater intrusion, Soil salinity

Increasing soil salinization is one of the most dominant environmental factors driving land degradation, affecting approximately 831 million hectares of land worldwide[1]. Salinization of agricultural lands has severe consequences for global food security, with studies documenting major declines in crop yields and reduced crop diversity[2–4]. Moreover, salinization imposes substantial economic burdens on agriculture, with annual losses estimated at $27 billion globally[5].

In addition to agricultural impacts, salt stress has been linked to the conversion and mortality of a variety of managed and natural coastal landscapes[6]. For example, saltwater intrusion has been observed to induce land use and land cover (LULC) changes, including conversion of farmland and bare soil to marshland owing to rising salinity[7,8]. Additionally, studies have reported the loss of upland forest[9], wetland forest[10], and mangroves[11]. These salinity-induced changes disrupt ecosystem services, threaten community livelihoods, and undermine ecological balance[12]. For instance, salinity has driven shifts toward more lucrative land uses, such as shrimp farming in rural Bangladesh, which offers considerably higher financial returns than traditional rice cultivation[13,14]. This situation is further compounded by accelerated sea-level rise (SLR), which converts coastal marshes and forests into open water, intensifying the challenge of preserving these critical ecosystems[9]. These transitions, such as upland forest retreat and freshwater wetland conversion, also lead to nutrient mobilization, highlighting the urgent need for effective salinity management, land cover monitoring, and climate adaptation strategies[15].

[1]Department of Geography and Spatial Sciences, University of Delaware, Newark, DE 19716, USA. [2]Department of Plant and Soil Sciences, University of Delaware, Newark, DE 19716, USA. [3]School of Life Sciences, Arizona State University, Tempe, AZ 85281, USA. [4]NASA Ames Research Center, Moffett Field, CA 94035, USA. [5]Bay Area Environmental Research Institute, Moffett Field, CA 94035, USA. ✉email: manansar@udel.edu

Soil salinization dynamics are site-specific and respond to external drivers through complex feedback mechanisms that balance resilience with increased vulnerability, shaped by both natural processes and human interventions[16]. These interactions, compounded by ecosystem and landscape characteristics that lag behind SLR rates, can extend the effects of SLR from decades to centuries[17,18]. This variability makes it challenging to monitor the impacts of salinization. For instance, a site might experience recurring hydroclimatic events driving salinization but could potentially recover if conditions such as drainage and freshwater input are favorable. An area experiencing high salinization for the first time may never recover and become uncultivable if unfavorable conditions, such as poor drainage and low freshwater input, hinder recovery from a storm surge with a high salt content (e.g., brackish water)[19]. However, negative feedback mechanisms can stabilize ecosystems during the early stages of salinity stress. These include reduced water use and resource competition in the surviving vegetation, soil accretion, and farmland management practices. Despite these stabilizing factors, processes that mitigate salinity, such as drainage improvements, can simultaneously increase hypoxia and other conditions that amplify saltwater intrusion and vegetation shifts once the critical thresholds are exceeded[20]. A notable consequence of such salinization episodes is LULC change, which can be either temporary or permanent depending on the nature of the event and site characteristics[9,21]. Such changes, influenced by a complex interplay of stabilizing and destabilizing feedback, are crucial for assessing a site's vulnerability to long-term salinization and for identifying mitigation and adaptation strategies for sustainable agriculture and socio-economic activities[19].

The mid-Atlantic, southeastern, and Gulf Coast regions of the United States of America (USA) are expected to face increasing challenges from saltwater intrusion and SLR exacerbated by climate change[8,22]. Understanding these changes is critical, especially because upland-to-wetland conversion disrupts both ecological and economic stability[8,23]. Marshes and mangroves, which replace inundated freshwater forests and farmlands, provide valuable ecosystem services such as reducing coastal erosion, improving water quality, protecting against storm surges, sequestering carbon, and providing marine habitats[24]. However, in the USA, residential property values may decrease in proximity to wetlands[25], making the conversion of uplands to wetlands undesirable for some[26]. Sustainable management in coastal regions requires adaptive strategies owing to shifting ecosystem boundaries and complex trade-offs between direct and indirect land-use values[27]. Spatial understanding of land vulnerable to varying degrees of salinization is thus essential for landowners and policymakers to improve decision-making.

Remote sensing techniques offer a valuable approach for mapping salinization dynamics and LULC, providing extensive temporal and spatial coverage that complements resource-intensive direct soil measurements, such as electrical conductivity (ECe)[28,29]. ECe, or the electrical conductivity of the saturation extract, is a widely accepted indicator of soil salinity, representing the concentration of soluble salts in water extracted from a saturated soil paste. Researchers have used a combination of remote sensing indices derived from multitemporal, multispectral, and hyperspectral imagery with biophysical data on soil properties to provide an accurate estimation of soil salinity changes using tools such as statistical regression models or machine learning algorithms[30–35]. The growing amount of high-resolution data from earth observation satellites[36], and state-of-the-art algorithms for land cover change detection[37,38] have made such Geographic Information Systems (GIS) and remote sensing techniques particularly suitable for understanding, analyzing, and monitoring LULC over large geographic regions in unprecedented detail.

In regions such as the Delmarva Peninsula (Fig. 1A; coastal counties in the states of Delaware, Maryland, and Virginia, USA), soil salinization poses a growing threat to LULC dynamics. Delmarva's economy is predominantly driven by agriculture and aquaculture, accounting for 28.4% of the total harvested farmland across the three states[8]. Consequently, increasing soil salinization threatens not only agricultural productivity but also land-use stability in a region where livelihoods are tightly coupled to coastal agroecosystems. Although numerous studies have explored soil salinity changes under various land-use conditions[39–41], the Delmarva region remains understudied in this context, leaving the nuanced interactions between salinization and LULC dynamics in coastal areas poorly understood. This study aims to address this gap by analyzing LULC changes on the Delmarva Peninsula for five years (2000, 2002, 2005, 2009, and 2016), matching the available surface salinity data from the Global Soil Salinity Map (GSSM) dataset (Fig. 1B[42]) and performing land cover classification using a Random Forest (RF) classifier (Fig. 2) by leveraging the daily synthetic surface reflectance of Landsat imagery derived from the Continuous Change Detection and Classification (CCDC) algorithm[43]. The GSSM dataset provides categorical salinity data for specific years across five salinity stages from non-saline to extremely saline. Integrating historical land cover data with soil salinity maps offers a cost-effective alternative to direct ECe measurement; and thus, can reveal long-term salinization trends and large-scale LULC changes often missed by field data. Accordingly, this study evaluates how salinity gradients influence land-use and land-cover dynamics by first quantifying the distribution of different land cover types across varying salinity levels, and then quantifying the loss/gain/stability in land covers within each salinity category. This study contributes to the growing body of knowledge on how salinization affects coastal ecosystems and offers insights into identifying priority areas for further monitoring in the face of increasing climate and anthropogenic pressures.

Results

Random Forest model performance

The RF classifier demonstrated strong performance in classifying the land cover classes across Delmarva, with overall training and testing accuracies of 100% and 90.6%, respectively. These results are further supported by the five-fold cross-validation accuracy of 90.2% ± 0.13% (Supplementary Table S1), which demonstrates consistent performance across different data subsets. Additionally, an OOB score of 90.3% provided independent validation of the model's predictive accuracy. High true positive counts are observed along the diagonal of the confusion matrix (Supplementary Fig. S2), reflecting accurate predictions across all land cover classes. Notably, forest, bare soil, and marsh exhibited excellent classification accuracy, with minimal misclassification into other categories. Water was classified with high accuracy, although minor confusion occurred with marsh areas, and

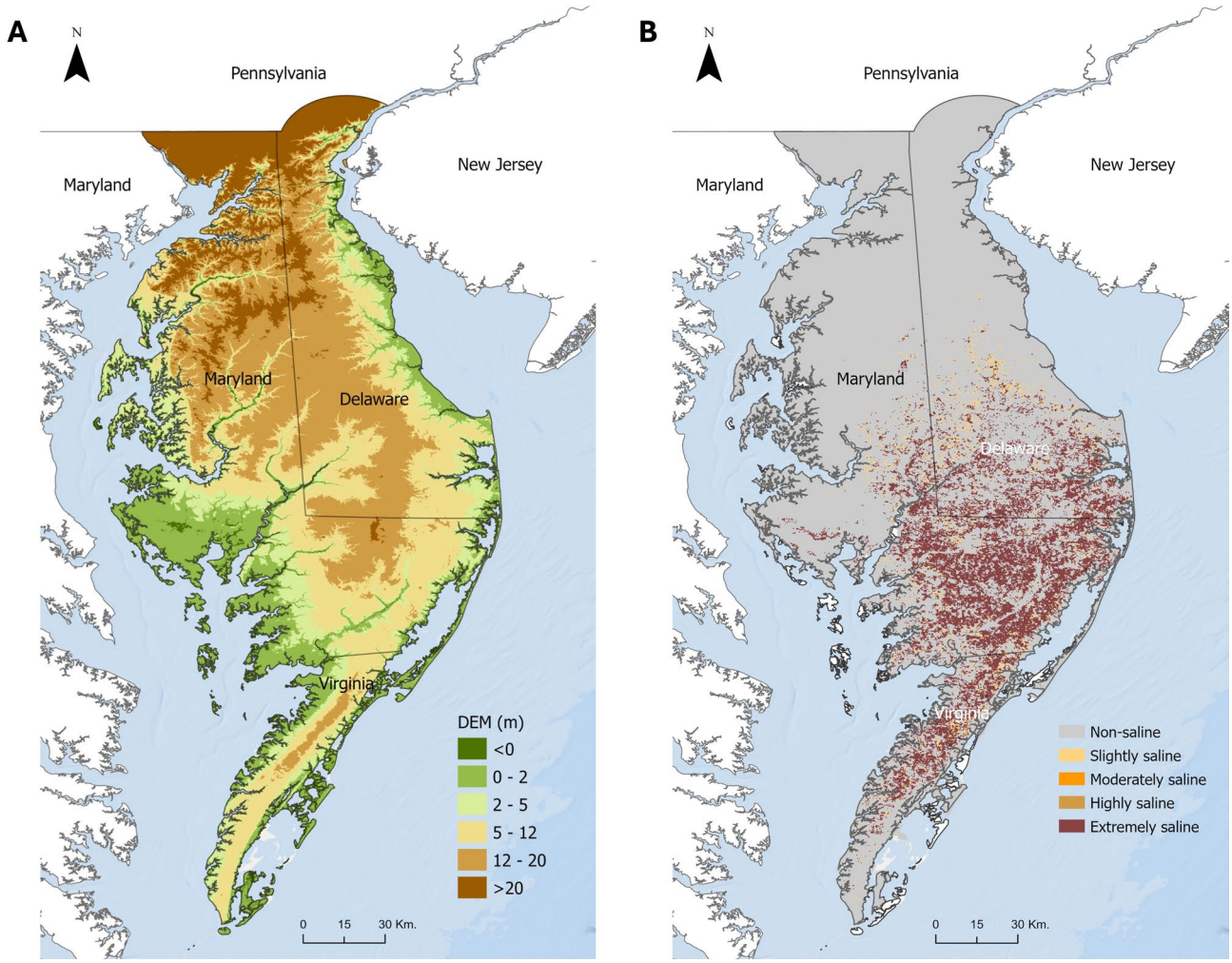

Fig. 1. Map of the study area, the Delmarva Peninsula, spanning 14 coastal counties of Delaware, Maryland, and Virginia. (A) Elevation above mean sea level, derived from the USGS 3DEP dataset and resampled to an 80 m resolution; (B) Global Soil Salinity Map for 2016 at 250 m resolution, classified into five salinity categories. The maps were created in ArcGIS Pro 3.6 (https://pro.arcgis.com/en/pro-app/latest/get-started/download-arcgis-pro.htm).

moderate confusion was observed between farmland and other vegetation classes. The model effectively captured the variability in the data, providing reliable classifications for most land cover types. Bare soil, built, forest, marsh and water achieved precision, recall, and F1-scores of approximately 0.90 or higher (Supplementary Fig. S2). Farmland and other vegetation showed slightly lower values for precision (0.82 for both), recall (0.87 and 0.81) and F1-scores (0.84 and 0.81). The macro-averaged precision, recall, and F1-score were all 0.91, indicating consistent performance across all classes.

Spatiotemporal changes in total area with varying salinity

From 2000 to 2016, Delmarva experienced notable fluctuations in areas with varying salinity. Most of the land (over 75%) in Delmarva was found to be non-saline (Salinity-0) across the study period, increasing by 1,138 km^2 (7.5%) during 2000–2016 (Table 1). Slightly saline areas (Salinity-1) peaked in 2002, but saw a drastic reduction by 2016, with a net loss of 342 km^2 (42%; Table 1). Extremely saline areas (Salinity-4) fluctuated but ultimately decreased by 833 km^2 (23%; Table 1). Moderate and highly saline areas (Salinity-2 and Salinity-3) remained minimal, with negligible changes across the study period.

The change detection maps (Fig. 3), illustrating the periods of 2000–2002, 2002–2005, 2005–2009, and 2009–2016, reveal a complex and regionally varied pattern of salinization. While both increases and decreases in salinity were observed across the peninsula over the study period, there was a prominent and recurrent pattern of this change along the coastal fringes and inland areas adjacent to the water bodies. While the Delmarva Peninsula experienced an increase in extremely saline (Salinity-4) regions during both 2000–2002 and 2005–2009 (Table 1), the spatial manifestation of this increase differed. Between 2000 and 2002, the expansion of extremely saline areas predominantly occurred in central inland regions. In contrast, from 2005 to 2009, the

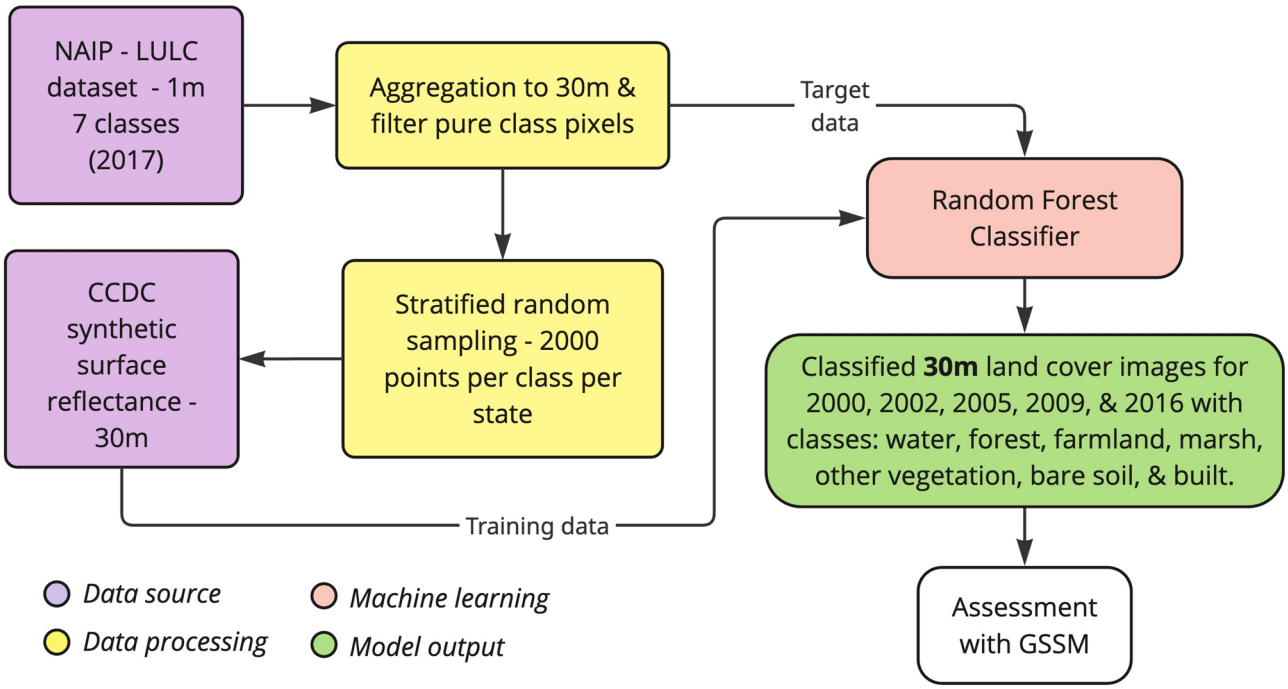

Fig. 2. Flowchart showing the datasets, data processing steps, and machine learning model used for land cover classification.

Year	Salinity-0	Salinity-1	Salinity-2	Salinity-3	Salinity-4
2000	15,081 (77%)	815 (4%)	1 (0%)	1 (0%)	3644 (19%)
2002	14,658 (75%)	889 (5%)	8 (0%)	4 (0%)	3943 (20%)
2005	15,979 (82%)	825 (4%)	2 (0%)	0 (0%)	2706 (14%)
2009	16,200 (83%)	61 (0%)	1 (0%)	0 (0%)	3274 (17%)
2016	16,219 (83%)	473 (2%)	1 (0%)	1 (0%)	2811 (14%)

Table 1. Land area (km^2) of various salinity classes over the years in Delmarva. Values in parentheses show the rounded percentage of area for each salinity zone out of the total land area (excluding water pixels) of the Delmarva Peninsula.

increase was primarily concentrated along coastal fringes (Fig. 3). These patterns suggest localized salinity responses to a combination of sea-level rise, hydrology, and land management dynamics.

Land cover distribution across salinity gradients

Our findings demonstrated that land cover categories exhibited uneven changes over time, with some showing consistent changes in salinity, while others experiencing fluctuations (Fig. 4). Across all classes, most land was found in the non-saline (Salinity-0) category, followed by varying extents of extremely saline (Salinity-4) and slightly saline (Salinity-1) zones between 2000 and 2016. The presence of land cover in the moderate (Salinity-2) and highly saline (Salinity-3) categories remained minimal. In terms of total area, forest exhibited the most substantial expansion, followed by other vegetation. In contrast, farmland and bare soil underwent noticeable declines, whereas marsh areas showed a modest decline.

Farmlands were predominantly in the non-saline category (Salinity-0) (Fig. 4), increasing slightly from 4,778 km^2 to 4,903 km^2 between 2000 and 2016. In contrast, the slightly saline (Salinity-1) farmland area declined sharply from 380 km^2 in 2000 to 186 km^2 in 2016. Additionally, the extremely saline (Salinity-4) farmland area decreased from 743 km^2 in 2000 to 525 km^2 in 2016. The loss of saline farmland area exceeded the gain in non-saline farmland, resulting in a net decline in total farmland area.

Other vegetation followed a similar salinity pattern overall (Fig. 4), with non-saline (Salinity-0) areas increasing from 2,475 km^2 in 2000 to 2,916 km^2 in 2016, indicating favorable conditions for growth and expansion over time. On the other hand, slightly saline (Salinity-1) and extremely saline (Salinity-4) other vegetation areas showed an overall decline to 125 km^2 and 487 km^2, respectively, by 2016. The total area for the other vegetation class increased, despite fluctuations across the salinity zones.

Marsh areas in the non-saline (Salinity-0) category increased from 2,171 km^2 to 2,192 km^2 between 2000 and 2016, with some fluctuations in between (Fig. 4). The slightly saline (Salinity-1) and extremely saline (Salinity-4)

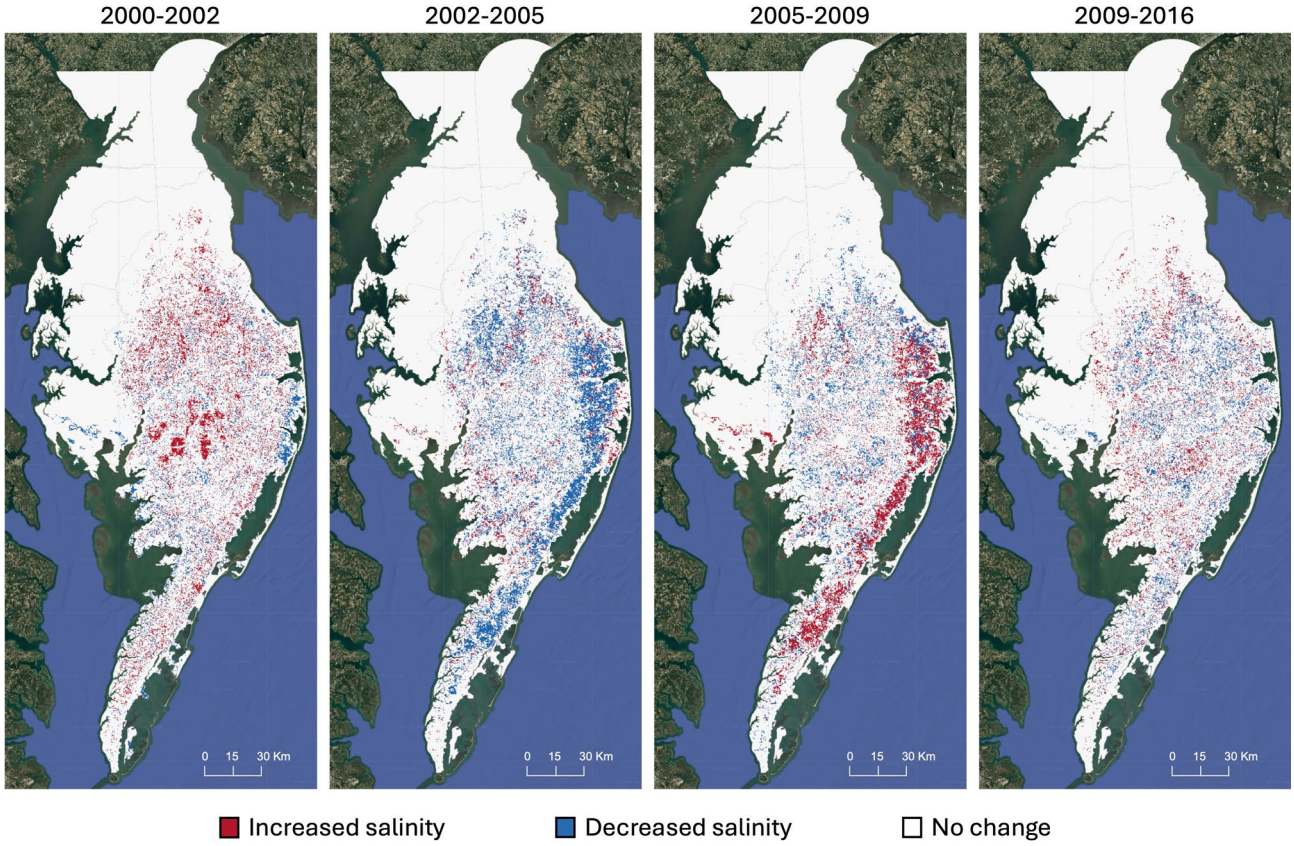

Fig. 3. Spatiotemporal evolution of salinity across the Delmarva Peninsula, 2000–2016. The maps show the dynamic patterns of salinization, with red indicating increased salinity, blue indicating decreased salinity, and white representing no change in salinity, across four distinct periods, 2000–2002, 2002–2005, 2005–2009, and 2009–2016. Each map was created on the Google Earth Engine code editor platform (https://code.earthengine.google.com/).

marsh areas showed a gradual decline from 15 km^2 to 6 km^2 and 220 km^2 to 68 km^2, respectively. Across these changes, the overall marsh area decreased throughout the study period.

The total bare soil area experienced a decline across all salinity categories during the study period (Fig. 4). Non-saline bare soil (Salinity-0) decreased from 429 km^2 to 187 km^2, slightly saline (Salinity-1) from 35 km^2 to 4 km^2, and extremely saline (Salinity-4) from 65 km^2 to 16 km^2 between 2000 and 2016.

The non-saline forest areas (Salinity-0) showed a net increase over the study period (Fig. 4), expanding from 4,527 km^2 in 2000 to 5,268 km^2 in 2016, following an initial decline in 2002. In contrast, forest areas affected by slight salinity (Salinity-1) rose to 300 km^2 by 2005 but subsequently declined to 130 km^2 by 2016. Extremely saline forest areas (Salinity-4) decreased from a peak of 2,107 km^2 in 2002 to 1,655 km^2 in 2016, indicating a reduction in the extent of saline forest over time.

Salinity dynamics across land cover change trajectories

Our analysis of salinity changes across land cover transitions revealed key aspects of landscape dynamics, highlighting land cover changes (Fig. 5A) and changes in salinity (unchanged, increased, and decreased) for each land cover that remained stable (Fig. 5B), were gained (Fig. 5C), and lost (Fig. 5D) between 2000 and 2016. Across all land cover transition categories, regardless of whether land cover remained stable, was gained, or lost, the majority of the area (> 83%) exhibited no change in salinity. A smaller proportion (7–11%) showed decreased salinity, whereas increases were rare, occurring in less than 5% of the area.

Between 2000 and 2016, farmland experienced a net loss primarily driven by the conversion of 1,007 km^2 to other vegetation. At the same time, farmland regained area through 604 km^2 converted from other vegetation and 252 km^2 from bare soil. Salinity trends across these transitions were largely stable, where 85–87% of areas showed no change, and 9–11% showed decreased salinity.

Other vegetation showed a net gain through dynamic exchanges with both farmland and forest. This change was primarily driven by inflow from farmland (1,007 km^2) and built-up areas (127 km^2), and outflow to forest (490 km^2) and farmland (604 km^2), with additional minor exchanges involving marsh and water categories. Salinity remained stable in 86–87% of these areas, and up to 10% experienced salinity reductions, indicating environmental conditions were broadly favorable for vegetative expansion.

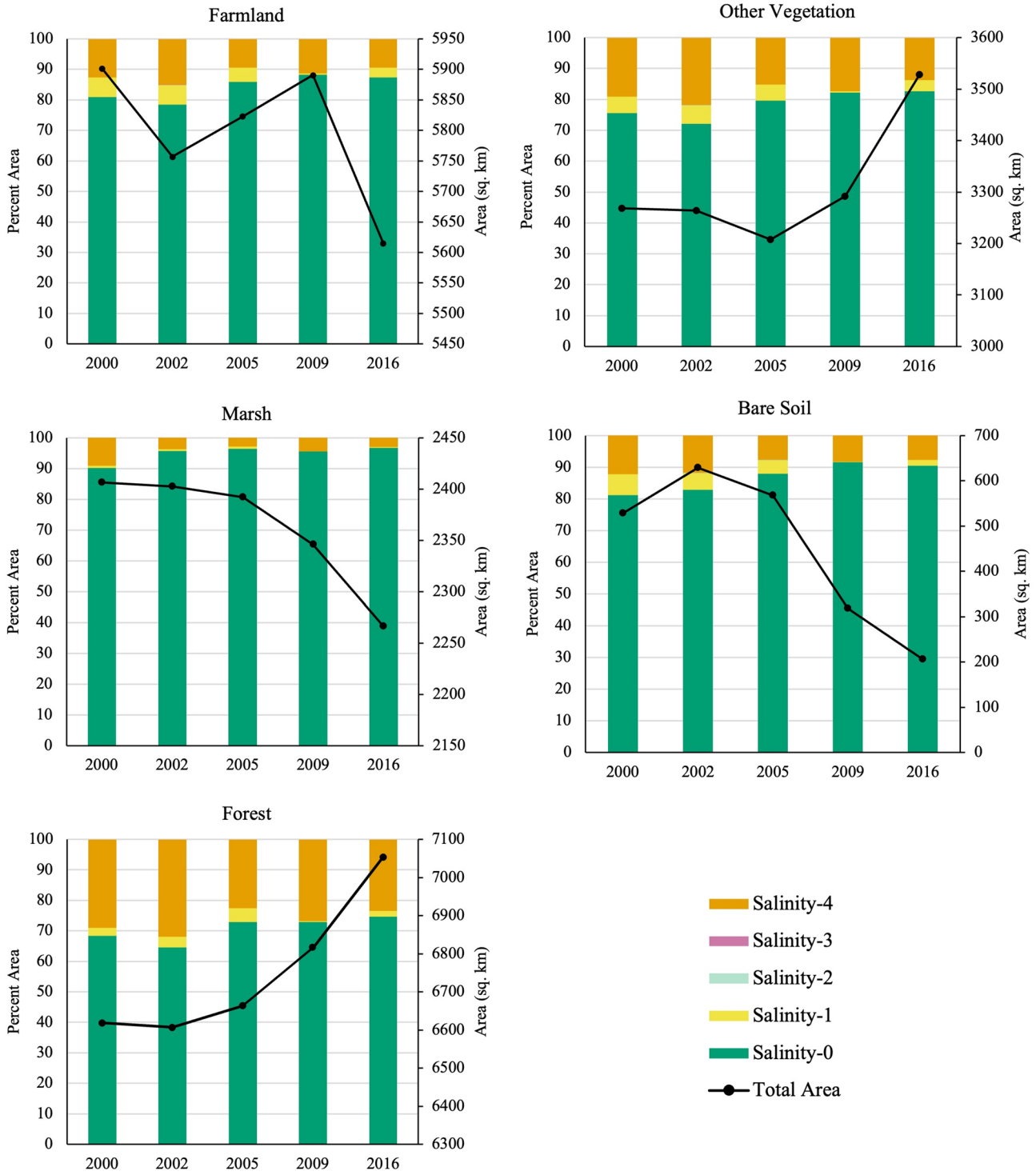

Fig. 4. Vertically stacked bar plots for each of the study years showing the proportion of total area across different salinity zones (primary y-axis). The black line represents the total area (secondary y-axis) for various land cover classes, including farmland, other vegetation, marsh, bare soil, and forest.

Marshes experienced a net decline, losing 360 km^2 mainly to water, farmland, and other vegetation, even after gaining 228 km^2 from reverse transitions. Despite this flux, salinity remained essentially unchanged in 85–90% of the marsh transitions, with 7–11% showing decreased salinity.

Bare soil declined considerably, primarily due to 252 km^2 transitioning to farmland in certain areas, even though 44 km^2 of farmland changed into bare soil. Salinity patterns showed high stability where stable bare soil retained the original salinity in 93% of the area, and other areas that gained or lost bare soil also showed strong stability (85–89%), with a modest decrease in salinity in 6–11% of the areas.

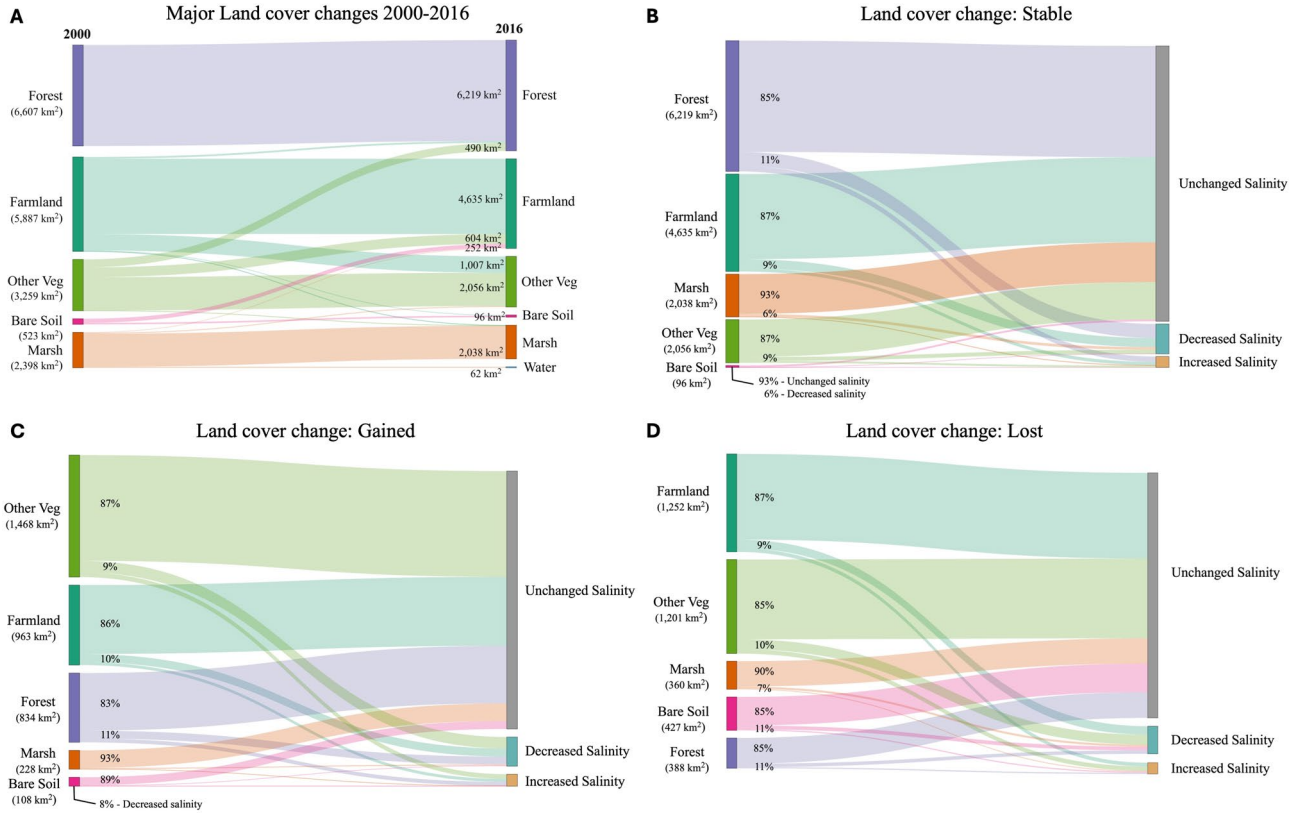

Fig. 5. Sankey diagrams summarizing land cover and salinity transitions between 2000 and 2016. (A) Major land cover changes across the study period. Labels on the left indicate total areas of each land cover in 2000, while those on the right highlight major transitions to other classes between 2000 and 2016. (B–D) Salinity change patterns for land covers that remained stable (B), were gained (C), or were lost (D) during the 2000–2016 period. For each land cover type, labels on the left show the percentage of area experiencing unchanged salinity and decreased salinity. Transitions representing less than 5% of the area—primarily those involving increased salinity—are not shown for clarity.

Forests saw the largest net increase in extent. Although 388 km^2 of forest was lost to different land covers, these were offset by 490 km^2 of gains from other vegetation and 111 km^2 from farmland, pointing to ongoing reforestation and natural regeneration. Salinity remained stable in 83–85% of forest transitions, with approximately 11% of areas showing decreased salinity, suggesting that changing salinity levels did not strictly constrain forest growth.

Discussion

This study demonstrates the value of pairing temporally consistent land cover classification with global salinity data. The CCDC-based approach used here offers a replicable framework for LULC classification, which further facilitates integration of existing multi-source data that are only available for certain years, such as GSSM. Our LULC classification, developed using a RF classifier, demonstrated high model reliability and strong generalization to unseen data, thus highlighting its robustness for large-scale applications. Examination of the confusion matrix revealed minor misclassification between water and marsh; this was anticipated given the spatial proximity and spectral similarity of these classes in the study area, a challenge also noted in similar coastal landscapes[44,45]. Similarly, moderate confusion between other vegetation and farmland is consistent with overlapping seasonal spectral characteristics common to these vegetation types as also seen in other coastal landscapes[46]. These patterns suggest that incorporating additional temporal or textural features can improve the class separability in future research[47,48].

Salinity fluctuations, particularly those in the extremely saline zones (Salinity-4), were not uniformly distributed across the peninsula. Instead, they were often found along coastal fringes or water-adjacent inland corridors, especially during 2005–2009 (Fig. 3). This spatial concentration is consistent with the mechanism of coastal saltwater intrusion, a process intensified by sea-level rise, increased intensity and frequency of high tides, and over extraction of groundwater[49–51]. A notable event is the tropical storm Ernesto in September 2006, which produced sharp salinity spikes along estuarine corridors[52], and triggered severe barrier island erosion in southern Delmarva[53], both creating pathways for saltwater encroachment onto adjacent low-lying areas.

Our findings also revealed a non-uniform relationship between land cover and salinity, with some classes exhibiting resilience, while others declining more sharply in saline environments. The year or season of satellite

or field observation might dictate the salinity level of a certain land cover, as it is not unusual for a region to go through a salinity spike after a coastal storm or flooding event, followed by a 'reduction' in salinity after a rainfall event. This likely explains why over 83% of each class, whether gained, lost or stable, retained its original salinity category from 2000 onward (Fig. 5). A small but consistent portion (7–11%) experienced decreased salinity that could simply represent the lower point of long-term fluctuations, or could be driven by enhanced salt leaching, improved pore structure, vegetation-driven salt uptake, and the application of organic or physical amendments, factors known to facilitate salinity decline under appropriate soil and climatic conditions[54]. Thus, the dominance of non-saline areas across all land cover classes, along with the decline in extremely and slightly saline zones (Fig. 4), highlights the potential value of more temporally frequent monitoring to better capture these dynamics.

These fluctuations in salinity and land cover contrast with those of more arid or semi-arid systems, where salinization is often a direct precursor to land abandonment and vegetation loss[55,56]. In Delmarva, resilience to salinity during land cover transitions may reflect the influence of active water and land management[57]. This was particularly evident in the reciprocal transitions between farmland and other vegetation. These transitions highlight that the relationship between land cover and salinity is not a one-way mechanism; rather, it is a dynamic feedback loop in which changes in land cover may influence salinity levels and vice versa. As land cover types shift, they can either contribute to or mitigate salinization processes, depending on various environmental, management, and climatic factors, as seen in semiarid and coastal landscapes[39,58,59]. For example, marsh vegetation might protect comparatively less salinized regions from further salt accumulation via salt uptake[60,61]. These findings suggest that examining transitions between land cover classes and their corresponding salinity levels could provide valuable insight into the processes driving land cover and salinity changes over time[19,41].

The farmland–non-crop (other) vegetation dynamic represents a highly active frontier of land cover change. Transitions from farmland to other vegetation are commonly associated with declining soil productivity or sub-surface waterlogging, both of which are well-documented precursors to land retirement[62,63]. However, our analysis reveals that this trend was not unidirectional. We observed that a considerable proportion of land cover initially classified as other vegetation was subsequently reclaimed as farmland. This indicates a hiatus rather than an irreversible conversion, likely representing periods of long-term fallow or rotational abandonment driven by soil conditions. Spatially, these reclamations coincided with areas of stable or decreasing salinity in the GSSM dataset. The increase in non-saline farmland areas over the study period suggests that land management or mitigation efforts may have been effective in these regions, contributing to the stability of these farmlands despite ongoing environmental pressures[19]. Additionally, the intermediate fluctuations in slightly and extremely saline farmland areas likely indicate episodic saltwater intrusion, hydrological variability, and targeted mitigation efforts[64–66].

The net decline in marshland over the study period mirrors well-documented patterns across the mid-Atlantic estuaries, where marshes are increasingly vulnerable to submergence due to sea-level rise, sediment deficits, and hydrodynamic alterations[67,68]. Conversions to open water and other vegetation point to a combination of geomorphic processes and anthropogenic pressures, including drainage, land reclamation, and development[69,70]. Conversely, transitions from open water or other vegetation back to marsh likely indicate recovery under more favorable hydrogeomorphic conditions and reduced anthropogenic pressure, which is consistent with marsh reestablishment when sediment supply and accommodation space are sufficient[71,72]. These nuances may warrant consideration in future land use planning or targeted marsh conservation efforts.

Methods

Study area

The Delmarva Peninsula is a relatively low-lying area, located on the eastern coast of the USA, with the majority of land below 20 m of elevation from sea level. It spans 14 coastal counties across the states of Delaware, Maryland, and Virginia (Fig. 1A). Delmarva is primarily characterized by forest, marshland, and farmland. Seafood, corn, and soybean production dominate agriculture and aquaculture in the region. Soil drainage varies across the region, with poorly drained soil found in lowland areas and well-drained soil in upland regions, which substantially influences hydrological processes and landscape dynamics[73].

Global soil salinity maps

The Global Soil Salinity Maps (GSSM; Fig. 1B) dataset is a moderate-resolution gridded dataset (spatial resolution: 250 m) developed by integrating seven soil property maps, thermal infrared imagery, and 15,188 ground truth points for electrical conductivity (ECe) from the World Soil Information Service (WoSIS) database[42]. The dataset categorizes soil salinity into five classes: non-saline (ECe < 2 dS/m), slightly saline (ECe 2–4 dS/m), moderately saline (ECe 4–8 dS/m), highly saline (ECe 8–16 dS/m), and extremely saline (ECe > 16 dS/m)[42]. The dataset offers an overall validation accuracy ranging from 67 to 70%. Here, we used GSSM for the years 2000, 2002, 2005, 2009, and 2016.

Land cover classification using Landsat time series data

The Continuous Change Detection and Classification (CCDC) algorithm was used to derive synthetic surface reflectance from Landsat imagery at daily time-steps for land cover classification. The CCDC is a powerful method for detecting and analyzing land surface changes over time by leveraging the full range of available Landsat data[43]. Changes were detected by comparing model predictions with satellite observations and flagging deviations beyond a set threshold within a moving time window (Supplementary Fig. S1). In this study, synthetic surface reflectance data from CCDC-derived Landsat imagery were used in two ways: (1) to identify stable land cover by analyzing the temporal consistency of surface reflectance, and (2) to extract spectral reflectance values from the first day of selected representative months, which were then used as inputs to an RF classifier for annual land cover classification from 2000 to 2016.

The CCDC-derived Landsat imagery was further complemented by a high-resolution National Agriculture Imagery Program (NAIP)-Landsat derived dataset of LULC for the year 2016–2017, with a spatial resolution of 1 m[74]. The NAIP-Landsat derived dataset was developed using 41,263 reference points, out of which 30% were used for accuracy assessment. The overall accuracy of this dataset is 83% for Virginia, 84% for Maryland, and 90% for Delaware[8]. This dataset was used to collect reference points for training the RF classifier after aggregating the individual LULC classes to 30 m to match the CCDC dataset (Fig. 2). Because NAIP images are not available for the entire contiguous U.S. (CONUS) for the same time-period, the dataset for the Delmarva region was as follows: Delaware – 3 counties – 2017, Maryland – 9 counties – 2017, and Virginia – 2 counties – 2016[74]. The NAIP-Landsat derived dataset offers 8 land cover classes: water, forest, farmland, marsh, other vegetation, bare soil, built, and salt patch, out of which we used 7 classes (all except salt patch). We used this dataset in two ways: (1) to identify pure pixels at 30 m spatial resolution, which were then used to extract the corresponding surface reflectance values from the CCDC dataset, and (2) to extract the labels for the pure pixels, which were used as target variables in the RF model training.

Reference data collection for RF model

The seven LULC classes from the NAIP-Landsat dataset were split into individual 1 m raster layers and aggregated to 30 m resolution in Google Earth Engine (GEE) using the 'count' reducer. Pixels with counts less than 900 (30×30) were masked out, retaining only pure land cover pixels for each class. To ensure reliable training data, we used only stable land cover pixels, those without abrupt changes one year before or after the classification year and those not in transitional states, such as degrading forests. Because NAIP imagery represents a single summer snapshot, we selected CCDC pixels that were stable over a three-year window to reduce misclassification. For Delaware and Maryland, stability was assessed from 2016 to 2018 (using NAIP 2017), and for Virginia from 2015 to 2017 (using NAIP 2016).

To identify stable pixels for training, we applied a threshold to the slope parameter from the CCDC dataset, which indicates the rate of spectral change over time and helps detect land cover transitions (Supplementary Fig. S1). Through random testing, pixels with slope values between − 0.005 and 0.005 in both the Red and NIR bands were considered stable, as these bands are most responsive to vegetation types relevant to salinization analysis (e.g., forest, farmland, and marsh). This yielded a mask of pixels with no abrupt change or transition between 2016 and 2018 for Delaware and Maryland, and 2015–2017 for Virginia. We applied this mask to the aggregated NAIP-Landsat land cover layers and performed stratified random sampling to select up to 2,000 stable points per land cover class per state for model training. The final distributions of training points are summarized in Supplementary Table S2.

To capture seasonal variability in land cover, we structured the CCDC preprocessing to include images from the first day of four representative months, January, April, July, and October, spanning winter to fall. This approach ensured that the training features reflected spectral variation relevant to the salinization dynamics. In addition to the standard Landsat bands (including blue, green, red, NIR, SWIR1, SWIR2, and thermal bands), we computed a set of spectral indices: Normalized Difference Vegetation Index (NDVI;[75], Normalized Burn Ratio (NBR;[76], Enhanced Vegetation Index (EVI;[77], and EVI2[78] (Supplementary Table S3). These indices highlight vegetation health, surface moisture, and other land cover characteristics that could be affected by salinization processes. We also applied the Tasseled Cap transformation[79] to derive brightness, greenness, and wetness indices, with greenness capturing vegetation cover and wetness and brightness providing insight into soil moisture retention. All features were stacked into a single multiband image, which served as the input for extracting sample values at training points for each land cover class. Processing was performed using the GEE, ensuring consistency and computational efficiency.

Random Forest classifier

A Random Forest (RF) classifier[80] was implemented in Python to perform LULC classification across seven classes: bare soil, built, farmland, forest, marsh, water, and other vegetation. RF was chosen for its robustness to noise, overfitting, and class imbalance, properties that make it well-suited for land cover mapping[81]. The algorithm builds an ensemble of decision trees using bootstrap samples, with the final prediction determined by the majority vote.

To ensure reliable classification results, the reference dataset was divided into a 70%-30% training and testing split, respectively and applied grid search with three-fold cross-validation to optimize the hyperparameters. The search tested combinations of n_estimators (50, 100, 200), max_depth (None, 10, 20, 30), min_samples_split (2, 5, 10), and min_samples_leaf (1, 2, 4). The grid search process, using three-fold cross-validation, systematically tested each possible parameter combination to determine the configuration that yielded the highest classification accuracy. The optimal parameter combination consisted of 100 trees ('n_estimators = 100'), an unlimited tree depth ('max_depth=None'), and standard minimum settings for splitting ('min_samples_split = 2') and leaf size ('min_samples_leaf = 1'). The robustness of the final model was evaluated using five-fold cross-validation and out-of-bag (OOB) scoring (Supplementary Table S1) to guard against overfitting. The five-fold cross-validation partitions the training data into five subsets, allowing the model to be iteratively trained on four subsets while validating on the remaining one, and OOB score is derived from the subset of data not used during the bootstrap sampling process in training. This offers a built-in measure of performance without relying on a separate validation set[82].

Model performance was assessed using precision, recall, and F1 score, computed using Scikit-learn's 'classification_report' function[83]. Precision measured the model's ability to reduce false positives, and recall captured its sensitivity to true positives. The F1 score, calculated as the harmonic mean of precision and recall, provided an overall measure of the model's performance in multivariable binary classification tasks. An F1 score of 1 indicates a perfect balance between precision and recall, whereas a score of 0 reflects poor model

performance. The resulting classified LULC maps were then combined with salinity layers to analyze how land cover types were distributed across salinity classes from 2000 to 2016, and to evaluate how salinity evolved across areas of land cover stability, loss, and gain. To address potential misalignments between the 30 m LULC data and the 250 m GSSM salinity data, we analyzed trends at the landscape scale rather than at the pixel scale. By aggregating land cover statistics within salinity zones, our objective was to minimize the impact of co-registration errors.

Caveats

Despite the strengths of the regional-scale analytical approach, the proposed framework has several limitations. The spatial resolution of the gridded soil salinity data may constrain the detection of fine-scale salinity heterogeneity within narrow marsh areas, agricultural drainage features, and land–water ecotones, where localized salinity thresholds can exert disproportionate influence on vegetation response. In addition, the CCDC framework prioritizes long-term temporal consistency, which may dampen short-duration salinity signals associated with episodic disturbances such as storm surge or extreme flooding events. Although the Random Forest classifier achieved high overall accuracy, residual spectral ambiguity among transitional land cover classes - particularly between marsh and open water and between farmland and other vegetation - introduces uncertainty in class-specific salinity attribution. Even though the RF classifier was trained using reference labels derived from the NAIP-Landsat fusion dataset for a single period (2016–2017), we only considered 'stable pixels' (as discussed in the "Reference data collection for RF model" sub-section), with minimal spectral change and land cover transitions during the adjacent years. This step ensured that the reference points used for training the RF model represented persistent land cover conditions rather than transitional states. While long-term shifts in agricultural practices, crop composition, or changing marsh vegetation structure may still influence class-specific spectral signatures over multi-decadal timescales, the use of spectrally stable training pixels provides confidence that the classifier captures the dominant and persistent characteristics of each land cover class. Future work could address this limitation by incorporating multi-year reference datasets, such as those acquired through earlier NAIP images or crowd-sourced validation data, to better constrain classification uncertainty across the entire study period. Furthermore, the absence of explicit socio-economic and land management information (e.g., drainage infrastructure, cropping decisions, land tenure, or management practices) limits direct attribution of observed land cover stability or recovery to specific human interventions. Finally, while strong spatial and temporal associations between land cover dynamics and salinity patterns are evident, the analysis does not establish causal relationships, as salinity interacts with hydrological processes, soil properties, management actions, and climate variability in complex ways that cannot be fully disentangled using snapshots of field or remotely sensed data.

Data availability

The multi-temporal land cover dataset for the Delmarva Peninsula (2000, 2002, 2005, 2009, 2016) at 30 m resolution are available via a public repository[84].

Received: 17 November 2025; Accepted: 20 March 2026
Published online: 27 March 2026

References

1. Daliakopoulos, I. N. et al. The threat of soil salinity: a European scale review. *Sci. Total Environ.* **573**, 727–739. https://doi.org/10.1016/j.scitotenv.2016.08.177 (2016).
2. Ahmed, Z. & Ambinakudige, S. Does land use change, waterlogging, and salinity impact on sustainability of agriculture and food security? Evidence from southwestern coastal region of Bangladesh. *Environ. Monit. Assess.* **195**, 74. https://doi.org/10.1007/s10661-022-10673-w (2022).
3. Mukhopadhyay, R., Sarkar, B., Jat, H. S., Sharma, P. C. & Bolan, N. S. Soil salinity under climate change: challenges for sustainable agriculture and food security. *J. Environ. Manag.* **280**, 111736 (2021).
4. Thitisaksakul, M. et al. Effects of timing and severity of salinity stress on rice (Oryza sativa L.) yield, grain composition, and starch functionality. *J. Agric. Food Chem.* **63**, 2296–2304. https://doi.org/10.1021/jf503948p (2015).
5. Qadir, M. et al. Economics of salt-induced land degradation and restoration. *Nat. Resour. Forum.* **38**, 282–295. https://doi.org/10.1111/1477-8947.12054 (2014).
6. Mondal, P., Sarupria, M. & Walter, M. A global review of the impacts of saltwater intrusion on soils and ecosystems. *Adv. Agron.* **191**, 2563. https://doi.org/10.1016/bs.agron.2025.01.002 (2025).
7. Fagherazzi, S. et al. Sea level rise and the dynamics of the marsh-upland boundary. *Front. Environ. Sci.* **7**, 25. https://doi.org/10.3389/fenvs.2019.00025 (2019).
8. Mondal, P. et al. The spread and cost of saltwater intrusion in the US Mid-Atlantic. *Nat. Sustain.* **6**, 1–11. https://doi.org/10.1038/s41893-023-01186-6 (2023).
9. Kirwan, M. L. & Gedan, K. B. Sea-level driven land conversion and the formation of ghost forests. *Nat. Clim. Chang.* **9**, 450–457. https://doi.org/10.1038/s41558-019-0488-7 (2019).
10. White, E. & Kaplan, D. Identifying the effects of chronic saltwater intrusion in coastal floodplain swamps using remote sensing. *Remote Sens. Environ.* **258**, 112385. https://doi.org/10.1016/j.rse.2021.112385 (2021).
11. Sippo, J. Z., Lovelock, C. E., Santos, I. R., Sanders, C. J. & Maher, D. T. Mangrove mortality in a changing climate: an overview. *Estuar. Coast Shelf Sci.* **215**, 241–249. https://doi.org/10.1016/j.ecss.2018.10.011 (2018).
12. Islam, R. et al. Salinity hazard drives the alteration of occupation, land use and ecosystem service in the coastal areas: evidence from the south-western coastal region of Bangladesh. *Heliyon* **9**, e18512. https://doi.org/10.1016/j.heliyon.2023.e18512 (2023).
13. Anik, A. R., Ranjan, R. & Ranganathan, T. Estimating the impact of salinity stress on livelihood choices and incomes in rural Bangladesh. *J. Int. Dev.* **30**, 1414–1438. https://doi.org/10.1002/jid.3364 (2018).
14. Belton, B. Shrimp, prawn and the political economy of social wellbeing in rural Bangladesh. *J. Rural Stud.* **45**, 230–242. https://doi.org/10.1016/j.jrurstud.2016.03.014 (2016).
15. Tully, K. et al. The invisible flood: the chemistry, ecology, and social implications of coastal saltwater intrusion. *BioScience* **69**, 368–378. https://doi.org/10.1093/biosci/biz027 (2019).

16. Armstrong, S. B. & Lazarus, E. D. Masked shoreline erosion at large spatial scales as a collective effect of beach nourishment. *Earth's Future*. **7**, 74–84. https://doi.org/10.1029/2018EF001070 (2019).
17. Kirwan, M. L. & Murray, A. B. Tidal marshes as disequilibrium landscapes? Lags between morphology and Holocene sea level change. *Geophys. Res. Lett.* **35**, 14523. https://doi.org/10.1029/2008GL036050 (2008).
18. Mariotti, G. & Hein, C. J. Lag in response of coastal barrier-island retreat to sea-level rise. *Nat. Geosci.* **15**, 633–638. https://doi.org/10.1038/s41561-022-00980-9 (2022).
19. Gibson, N. et al.Identification, mitigation, and adaptation to salinization on working lands in the U.S. Southeast. General Technical Report SRS-259, 1–69; 10.2737/SRS-GTR-259 (U.S. Department of Agriculture Forest Service, Southern Research Station) (2021).
20. Kirwan, M. L. et al. Feedbacks regulating the salinization of coastal landscapes. *Annu. Rev. Mar. Sci.* **17**, 461–484. https://doi.org/10.1146/annurev-marine-070924-031447 (2024).
21. Magolan, J. L. & Halls, J. N. A multi-decadal investigation of tidal creek wetland changes, water level rise, and ghost forests. *Remote Sens.* **12**, 1141. https://doi.org/10.3390/rs12071141 (2020).
22. O'Donnell, K. L. et al. Saltwater intrusion and sea level rise threatens U.S. rural coastal landscapes and communities. *Anthropocene* **45**, 100427. https://doi.org/10.1016/j.ancene.2024.100427 (2024).
23. Guimond, J. A. & Michael, H. A. Effects of marsh migration on flooding, saltwater intrusion, and crop yield in coastal agricultural land subject to storm surge inundation. *Water Resour. Res.* **57**, WR028326. https://doi.org/10.1029/2020WR028326 (2021).
24. Barbier, E. B. et al. The value of estuarine and coastal ecosystem services. *Ecol. Monogr.* **81**, 169–193. https://doi.org/10.1890/10-1510.1 (2011).
25. Field, C. R., Dayer, A. A. & Elphick, C. S. Landowner behavior can determine the success of conservation strategies for ecosystem migration under sea-level rise. *Proc. Natl Acad. Sci. USA* **114**, 9134–9139. https://doi.org/10.1073/pnas.1620319114 (2017).
26. Bin, O. & Polasky, S. Evidence on the amenity value of wetlands in a rural setting. *J. Agric. Appl. Econ.* **37**, 589–602. https://doi.org/10.1017/S1074070800027103 (2005).
27. Feagin, R. A., Martinez, M. L., Mendoza-Gonzalez, G. & Costanza, R. Salt marsh zonal migration and ecosystem service change in response to global sea level rise: a case study from an urban region. *Ecol. Soc.* **15**, 14. https://doi.org/10.5751/ES-03724-150414 (2010).
28. Sahbeni, G., Ngabire, M., Musyimi, P. K. & Székely, B. Challenges and opportunities in remote sensing for soil salinization mapping and monitoring: a review. *Remote Sens.* **15**, 2540. https://doi.org/10.3390/rs15102540 (2023).
29. Allbed, A. & Kumar, L. Soil salinity mapping and monitoring in arid and semi-arid regions using remote sensing technology: a review. *Adv. Remote Sens.* **2**, 373–385. https://doi.org/10.4236/ars.2013.24040 (2013).
30. Al-Khaqani, E., Shneen, W., Yousif, S. R. & Al-Kazaali, H. Using Landsat 8 OLI data to predict and mapping soil salinity for part of An-Najaf governorate. *Ecol. Environ. Conserv.* **24**, 572–578 (2017).
31. Alqasemi, A. S. et al. Detection and modeling of soil salinity variations in arid lands using remote sensing data. *Open. Geosci.* **13**, 443–453. https://doi.org/10.1515/geo-2020-0244 (2021).
32. Bai, L. et al. Remote sensing of soil alkalinity and salinity in the Wuyu'er-Shuangyang River Basin, Northeast China. *Remote Sens.* **8**, 163. https://doi.org/10.3390/rs8020163 (2016).
33. Davis, E., Wang, C. & Dow, K. Comparing Sentinel-2 MSI and Landsat 8 OLI in soil salinity detection: a case study of agricultural lands in coastal North Carolina. *Int. J. Remote Sens.* **40**, 6134–6153. https://doi.org/10.1080/01431161.2019.1587205 (2019).
34. Hassani, A., Azapagic, A. & Shokri, N. Global predictions of primary soil salinization under changing climate in the 21st century. *Nat. Commun.* **12**, 6663. https://doi.org/10.1038/s41467-021-26907-3 (2021).
35. Scudiero, E. et al. Remote sensing is a viable tool for mapping soil salinity in agricultural lands. *Calif. Agric.* **71**, 231–238. https://doi.org/10.3733/ca.2017a0009 (2017).
36. Belward, A. S. & Skøien, J. O. Who launched what, when and why; trends in global land-cover observation capacity from civilian earth observation satellites. *ISPRS J. Photogramm. Remote Sens.* **103**, 115–128. https://doi.org/10.1016/j.isprsjprs.2014.03.009 (2015).
37. Woodcock, C. E., Loveland, T., Herold, M. & Bauer, M. E. Transitioning from change detection to monitoring with remote sensing: a paradigm shift. *Remote Sens. Environ.* **238**, 111558. https://doi.org/10.1016/j.rse.2019.111558 (2020).
38. Zhu, Z. Change detection using landsat time series: a review of frequencies, preprocessing, algorithms, and applications. *ISPRS J. Photogramm. Remote Sens.* **130**, 370–384. https://doi.org/10.1016/j.isprsjprs.2017.06.013 (2017).
39. Pessoa, L. G. M. et al. Assessment of soil salinity status under different land-use conditions in the semiarid region of Northeastern Brazil. *Ecol. Indic.* **141**, 109139. https://doi.org/10.1016/j.ecolind.2022.109139 (2022).
40. Saad, K., Kallel, A., Rebah, Z. B. & Solaiman, B. Spatio-temporal monitoring of soil salinity and land cover changes using remote sensing techniques: Zaghouan case study (Tunisia). In *2022 6th International Conference on Advanced Technologies for Signal and Image Processing (ATSIP)* 1–5 (IEEE, 2022). https://doi.org/10.1109/ATSIP55956.2022.9805954.
41. Thiam, S. et al. Monitoring land use and soil salinity changes in coastal landscape: a case study from Senegal. *Environ. Monit. Assess.* **193**, 2563. https://doi.org/10.1007/s10661-021-08958-7 (2021).
42. Ivushkin, K. et al. Global mapping of soil salinity change. *Remote Sens. Environ.* **231**, 111260. https://doi.org/10.1016/j.rse.2019.111260 (2019).
43. Zhu, Z. & Woodcock, C. E. Continuous change detection and classification of land cover using all available Landsat data. *Remote Sens. Environ.* **144**, 152–171. https://doi.org/10.1016/j.rse.2014.01.011 (2014).
44. Gallant, A. The challenges of remote monitoring of wetlands. *Remote Sens.* **7**, 10938–10950. https://doi.org/10.3390/rs70810938 (2015).
45. Mahdavi, S. et al. Remote sensing for wetland classification: a comprehensive review. *GISci Remote Sens.* **55**, 623–658. https://doi.org/10.1080/15481603.2017.1419602 (2018).
46. Torbick, N. & Salas, W. Mapping agricultural wetlands in the Sacramento Valley, USA with satellite remote sensing. *Wetl. Ecol. Manag.* **23**, 79–94. https://doi.org/10.1007/s11273-014-9342-x (2014).
47. Jia, K. et al. Land cover classification of Landsat data with phenological features extracted from time series MODIS NDVI data. *Remote Sens.* **6**, 11518–11532. https://doi.org/10.3390/rs61111518 (2014).
48. Müller, H., Rufin, P., Griffiths, P., Barros Siqueira, A. J. & Hostert, P. Mining dense Landsat time series for separating cropland and pasture in a heterogeneous Brazilian savanna landscape. *Remote Sens. Environ.* **156**, 490–499. https://doi.org/10.1016/j.rse.2014.10.014 (2015).
49. Eswar, D., Karuppusamy, R. & Chellamuthu, S. Drivers of soil salinity and their correlation with climate change. *Curr. Opin. Environ. Sustain.* **50**, 310–318. https://doi.org/10.1016/j.cosust.2020.10.015 (2021).
50. Peters, C. N. et al. Groundwater pumping causes salinization of coastal streams due to baseflow depletion: analytical framework and application to Savannah River, GA. *J. Hydrol.* **604**, 127238. https://doi.org/10.1016/j.jhydrol.2021.127238 (2022).
51. Werner, A. D. & Simmons, C. T. Impact of sea-level rise on sea water intrusion in coastal aquifers. *Groundwater* **47**, 197–204. https://doi.org/10.1111/j.1745-6584.2008.00535.x (2009).
52. Maryland Department of Natural Resources. Impact of Tropical Storm Ernesto and subsequent rain event (September 2006). In *Eyes on the Bay*. https://eyesonthebay.dnr.maryland.gov/eyesonthebay/stories2/sept_rains_2006.html (2006).
53. Nebel, S. H., Trembanis, A. C. & Barber, D. C. Tropical cyclone frequency and barrier island erosion rates, Cedar Island, Virginia. *J. Coast Res.* **29**, 133–144. https://doi.org/10.2112/JCOASTRES-D-11-00206.1 (2013).
54. Shaygan, M. & Baumgartl, T. Reclamation of salt-affected land: a review. *Soil. Syst.* **6**, 61. https://doi.org/10.3390/soilsystems6030061 (2022).

55. Rengasamy, P. World salinization with emphasis on Australia. *J. Exp. Bot.* **57**, 1017–1023. https://doi.org/10.1093/jxb/erj108 (2006).
56. Zhao, L., Yang, Q., Zhao, Q. & Wu, J. Assessing the long-term evolution of abandoned salinized farmland via temporal remote sensing data. *Remote Sens.* **13**, 4057. https://doi.org/10.3390/rs13204057 (2021).
57. Sudol, T. A., Hesed, M., Clark, C. D., Moser, F. C. & J. M. & Resisting-accepting-directing sea level rise on the Chesapeake Bay: agricultural producers' motivations and actions. *J. Environ. Manag.* **332**, 117355. https://doi.org/10.1016/j.jenvman.2023.117355 (2023).
58. Sternberg, L. D. S. L., Teh, S. Y., Ewe, S. M. L., Miralles-Wilhelm, F. & DeAngelis, D. L. Competition between hardwood hammocks and mangroves. *Ecosystems* **10**, 648–660. https://doi.org/10.1007/s10021-007-9050-y (2007).
59. Wendelberger, K. S. & Richards, J. H. Halophytes can salinize soil when competing with glycophytes, intensifying effects of sea level rise in coastal communities. *Oecologia* **184**, 729–737. https://doi.org/10.1007/s00442-017-3896-2 (2017).
60. Poulter, B., Christensen, N. L. & Qian, S. S. Tolerance of Pinus taeda and Pinus serotina to low salinity and flooding: implications for equilibrium vegetation dynamics. *J. Veg. Sci.* **19**, 15–22. https://doi.org/10.3170/2007-8-18410 (2008).
61. de Barros, P. R. D., Schulenburg, A. N., Gedan, K., Miller, C. & Tully, K. L. Effects of saltwater intrusion on candidate restoration species in coastal agricultural fields. *Agric. Ecosyst. Environ.* **392**, 109757. https://doi.org/10.1016/j.agee.2025.109757 (2025).
62. Lal, R. Soil degradation by erosion. *Land. Degrad. Dev.* **12**, 519–539. https://doi.org/10.1002/ldr.472 (2001).
63. Perpiña Castillo, C., Jacobs-Crisioni, C., Diogo, V. & Lavalle, C. Modelling agricultural land abandonment in a fine spatial resolution multi-level land-use model: an application for the EU. *Environ. Model. Softw.* **136**, 104946. https://doi.org/10.1016/j.envsoft.2020.104946 (2021).
64. Cantelon, J. A., Guimond, J. A., Robinson, C. E., Michael, H. A. & Kurylyk, B. L. Vertical saltwater intrusion in coastal aquifers driven by episodic flooding: a review. *Water Resour. Res.* **58**, WR032614. https://doi.org/10.1029/2022WR032614 (2022).
65. Li, D., Liu, B., Lu, Y. & Fu, J. The characteristic of compound drought and saltwater intrusion events in the several major river estuaries worldwide. *J. Environ. Manag.* **350**, 119659. https://doi.org/10.1016/j.jenvman.2023.119659 (2024).
66. Tarolli, P., Luo, J., Park, E., Barcaccia, G. & Masin, R. Soil salinization in agriculture: mitigation and adaptation strategies combining nature-based solutions and bioengineering. *iScience* **27**, 108830. https://doi.org/10.1016/j.isci.2024.108830 (2024).
67. Kirwan, M. L. & Megonigal, J. P. Tidal wetland stability in the face of human impacts and sea-level rise. *Nature* **504**, 53–60. https://doi.org/10.1038/nature12856 (2013).
68. Ohenhen, L. O., Shirzaei, M., Ojha, C. & Kirwan, M. L. Hidden vulnerability of US Atlantic coast to sea-level rise due to vertical land motion. *Nat. Commun.* 14, 2038. https://doi.org/10.1038/s41467-023-37853-7 (2023).
69. Ganju, N. K. et al. Spatially integrative metrics reveal hidden vulnerability of microtidal salt marshes. *Nat. Commun.* **8**, 14156. https://doi.org/10.1038/ncomms14156 (2017).
70. Weston, N. B. Declining sediments and rising seas: an unfortunate convergence for tidal wetlands. *Estuaries Coasts.* **37**, 1–23. https://doi.org/10.1007/s12237-013-9654-8 (2014).
71. Kirwan, M. L., Walters, D. C., Reay, W. G. & Carr, J. A. Sea level driven marsh expansion in a coupled model of marsh erosion and migration. *Geophys. Res. Lett.* **43**, 4366–4373. https://doi.org/10.1002/2016GL068507 (2016).
72. Schieder, N., Walters, D. & Kirwan, M. Massive upland to wetland conversion compensated for historical marsh loss in Chesapeake Bay, USA. *Estuaries Coasts.* **41**, 940–951. https://doi.org/10.1007/s12237-017-0336-9 (2018).
73. Lowrance, R. et al. Water quality functions of riparian forest buffers in Chesapeake Bay watersheds. *Environ. Manag.* **21**, 687–712. https://doi.org/10.1007/s002679900060 (1997).
74. Mondal, P. et al. High-resolution remotely sensed datasets for saltwater intrusion across the Delmarva Peninsula. *Zenodo* https://doi.org/10.5281/zenodo.6685695 (2022).
75. Rouse, J. W. Jr., Haas, R. H., Schell, J. A. & Deering, D. W. Monitoring vegetation systems in the Great Plains with ERTS. *NASA Spec. Publ* **351**, 309 (1974).
76. Key, C. H. & Benson, N. C. Landscape Assessment (LA). In *2006: FIREMON: Fire effects monitoring and inventory system* (eds. Lutes, D. C. et al.) Gen. Tech. Rep. RMRS-GTR-164-CD. Fort Collins, CO: U.S. Department of Agriculture, Forest Service, Rocky Mountain Research Station. LA-1-55 164 (2006).
77. Huete, A. et al. Overview of the radiometric and biophysical performance of the MODIS vegetation indices. *Remote Sens. Environ.* **83**, 195–213 (2002).
78. Jiang, Z., Huete, A. R., Didan, K. & Miura, T. Development of a two-band enhanced vegetation index without a blue band. *Remote Sens. Environ.* **112**, 3833–3845. https://doi.org/10.1016/j.rse.2008.06.006 (2008).
79. Crist, E. P. A TM Tasseled Cap equivalent transformation for reflectance factor data. *Remote Sens. Environ.* **17**, 301–306 (1985).
80. Breiman, L. Random forests. *Mach. Learn.* **45**, 5–32. https://doi.org/10.1023/A:1010933404324 (2001).
81. Belgiu, M. & Drăguț, L. Random forest in remote sensing: a review of applications and future directions. *ISPRS J. Photogramm. Remote Sens.* **114**, 24–31. https://doi.org/10.1016/j.isprsjprs.2016.01.011 (2016).
82. James, G., Witten, D., Hastie, T. & Tibshirani, R. An Introduction to Statistical Learning: with applications in R. *Springer Texts Stat.* https://doi.org/10.1007/978-1-0716-1418-1 (2021).
83. Blagec, K., Dorffner, G., Moradi, M. & Samwald, M. A critical analysis of metrics used for measuring progress in artificial intelligence. *arXiv* https://doi.org/10.48550/arXiv.2008.02577 (2020). 2008.02577.
84. Sarupria, M., Mondal, P., Park, T. & Vargas, R. Multi-temporal land cover dataset for the Delmarva Peninsula (2000, 2002, 2005, 2009, 2016) at 30 m resolution. *Zenodo* https://doi.org/10.5281/zenodo.16783114 (2025).

Acknowledgements

We are grateful for the logistical support provided by the Eastern Shore Land Conservancy and Dr. Kate Tully's research group at the University of Maryland during field data collection.

Author contributions

M.S. conceived the study, carried out the primary research, collected and processed the data, developed the models, and wrote the main manuscript text. R.V., T.P., and P.M. contributed to the development of the methodological framework, supervising and providing critical feedback on the manuscript. T.P. provided technical guidance and training on specialized methods. All authors reviewed the manuscript, contributed to revisions, and approved the final version for publication.

Funding

This work was supported by the National Aeronautics and Space Administration EPSCoR Grant DE-80NSSC20M0220 awarded to P.M. and R.V. We acknowledge the financial support provided to P.M. by the State of Maryland and Harry R. Hughes Center for Agro-Ecology. P.M. and M.S. were partially supported by the National Science Foundation EPSCoR Grant Award: Collaborative Research: RII FEC: Risks, Impacts, & Strategies for Coastal Communities: Advancing Convergent Science to Support Climate Change Adaptation & Resilience,

Award #s: 2418394, 2418395, 2418396.

Competing interests
The authors declare no competing interests.

Additional information
Supplementary Information The online version contains supplementary material available at https://doi.org/10.1038/s41598-026-45611-0.

Correspondence and requests for materials should be addressed to M.S.

Reprints and permissions information is available at www.nature.com/reprints.

Publisher's note Springer Nature remains neutral with regard to jurisdictional claims in published maps and institutional affiliations.